IEEE Access
Multidisciplinary | Rapid Review | Open Access Journal

Received 11 November 2022, accepted 27 November 2022, date of publication 1 December 2022,
date of current version 7 December 2022.

*Digital Object Identifier 10.1109/ACCESS.2022.3226261*

RESEARCH ARTICLE

# Structured Analysis and Review of Filter-Based Control Strategies for Hybrid Energy Storage Systems

**SEBASTIAN GÜNTHER[1], LEONHARD WEBER[2], ASTRID L. BENSMANN[1], AND RICHARD HANKE-RAUSCHENBACH[1]**

[1]Institute of Electric Power Systems, Leibniz University Hannover, 30167 Hannover, Germany
[2]Faculty of Mechanical Engineering, Leibniz University Hannover, 30823 Garbsen, Germany

Corresponding author: Astrid L. Bensmann (astrid.bensmann@ifes.uni-hannover.de)

This work was supported in part by the German Federal Ministry of Education and Research [Bundesministerium für Bildung und Forschung (BMBF)] under Grant 03SF0560A, and in part by the Open Access Fund of Leibniz University Hannover.

**ABSTRACT** Hybrid energy storage systems (HESS), i.e., the combination of two different energy storage technologies, are widely discussed as a promising solution for energy storage problems. A common control scheme to allocate the power between these storages and the subject of this study is filter-based control, where a filter splits the input signal into a low-frequency and high-frequency part. It provides robust results and easy implementation, although more advanced strategies may perform better. Many publications use this controller for specific problems, but a structured analysis of this controller type that quantifies the advantages and disadvantages, traits, and setbacks is missing. This work fills this gap and structures, summarizes, and provides mathematical background and guidelines on filter-based control of hybrid energy storage systems. Numerical simulations are performed to quantify the impact of design variables, parameters, or the input signal by using a linear storage model with efficiency and self-discharge rate and a low-pass filter controller with constant energy feedback as a representative subtype of this control scheme. The present work proves the high cycle-reduction capabilities of filter-controlled HESS at the cost of overdimensioning compared to more advanced control strategies. It demonstrates that using a high-efficiency, high-power storage with a low self-discharge rate and high-energy storage leads to smaller overall dimensioning and losses than a single storage system. The study identifies the feedback factor of the controller as the most impacting design variable.

**INDEX TERMS** Energy management, energy storage, hybrid energy storage systems, low-pass filters, power control, simulation, statistical analysis, systems modeling.

## I. INTRODUCTION

The subject of the present work is the investigation of filter-based control strategies for hybrid energy storage systems (HESS). A HESS combines two different energy storage technologies into a single storage system to increase the performance of the overall storage system, decrease costs and dimensions and increase the overall system's lifetime, efficiency, and response time. It is mandatory for a proper functioning HESS that the power is distributed correctly between the two storage technologies, i.e., the control strategy or energy management the HESS operates with is crucial [1], [2], [3], [4], [5], [6], [7], [8], [9]

There are various classes of control schemes for HESS: rule-based or fuzzy-logic-based control, filter-based control, online (model predictive) and offline optimization-based control or control with the help of neural networks [1], [4], [5], [6], [7], [8], [10], [11]. Note that this study deals with control as an energy management strategy that allocates the power flow to and between the two storages at a system level. It does not deal with closed-loop control at the implementation level, eliminating the error between a setpoint and the

The associate editor coordinating the review of this manuscript and approving it for publication was Lei Wang.

actual state at a current or voltage level. I.e., common linear proportional-integral control (e.g. [11]), two-point control (e.g. [11]), or advanced and robust control such as (adaptive terminal) sliding mode control (e.g. [12], [13], [14], [15]), observer-based control (e.g. [16], [17]), variable voltage control (e.g. [18]) or droop control (e.g. [11]), that all have been introduced for HESS, do not fall into the introduced categorization and scope of the analysis. Moreover, the present study makes no assumptions on the architecture of the storage system or controller implementation, i.e., Single-Hess vs. Multi-HESS or centralized vs. distributed control (e.g. [19], [20]).

Filter-based control is an extensive subset within the different control paradigms, and it is widely implemented [9], [21], [22], [23], [24]. It is relatively simple but offers robust performance and achieves good results on dynamics and cycle reduction [9], [21], [22], [25], [26], [27], [28]. There is no explicit or generalized analysis of the design of filter-based control strategies, although it is often implemented and used in case studies (e.g. [21], [22], [23], [25], [27], [28], [29], [30], [31], [32], [33]), Either the choice of values of design variables of this controller type is undocumented (e.g. [25], [26], [27], [33], [34], [35]), or it is a consequence of a (meta-)heuristic optimization (e.g. [22], [32], [36], [37], [38]). The influence and sensitivity of these design variables or the influence of other parameters, such as the input power profile, on the performance of the filter-based control are not investigated holistically. It is left unanswered how, when, and in which cases it is reasonable to use a HESS with filter-based control. Mentionable previous work is done in [21], which also studies the aspects of overdimensioning and losses for filter-controlled HESS and identifies phase shift and unnecessary energy exchange as a source. However, this work falls short of investigating multiple design parameters besides the filter's cutoff frequency and multiple characteristics and derives results from only one case study. In [9], different kinds of filter-based control are reviewed, and the performance is evaluated and compared in a case study, but it falls short of providing sufficient verification and analysis on the design parameters, too. A more thorough discussion and review on filter-based control will follow in Section II.

The present study aims to find and generalize insights from previous case studies for filter-based control strategies for HESS and back them up through numerical experiments, extensive and structured parameter studies, and statistical analysis. The study includes the investigation of the influence of control parameters and the choice of the input signal and storage parameters. Also, the study presents condensed advice and conclusions when designing and choosing a filter-based controller for HESS. Specifically, this includes answering the following research questions:

- How do design parameters such as feedback factor or cutoff frequency influence characteristics such as dimensions, losses, cycles, or dynamic stress of the individual storages?
- How do load profile characteristics, such as mean value or frequency spectrum, influence the above characteristics?
- How do storage parameters such as efficiency or self-discharge rate influence the above characteristics?

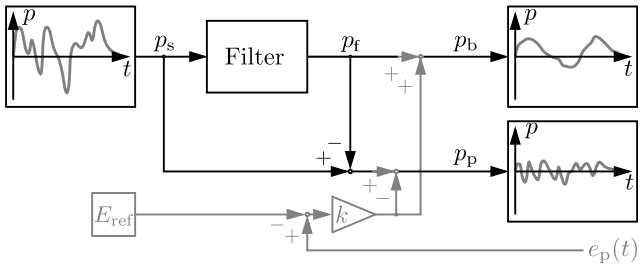


**FIGURE 1. General layout of filter-based control strategies. An input signal with a broad frequency spectrum is low-pass filtered, and the controller feeds the result to the first storage and the difference between the input and filtered signal to the second storage. Most implementations utilize an additional state of charge feedback loop for the second storage (shown in gray).**

The following Section II provides a literature review on filter-based control strategies. Section III covers the used model and methodology and introduces output characteristics of interest. Section IV defines a reference case with reference input and a reference parameter set for the storages and the controller. The section also presents and detailly describes arising results. Section V extends the previous elaborations by introducing parameter variations of the input signal, the storage model, and the control strategy. Section VI gathers insights from the generated data, extracts results, and derives key findings and design guidelines. Section VII summarizes the paper.

## II. REVIEW ON FILTER-BASED CONTROL FOR HESS

Filter-based control strategies are the focus of this study. Fig. 1 shows the typical structure of this controller type. The first step discusses only the open loop behavior without the gray feedback branch. The filter splits the input signal $p_s$ for a single storage into a low-frequency signal $p_b$ and a high-frequency signal $p_p$, which is the difference between the input signal and low-frequency signal. This implementation is the most straightforward but exposes poor performance, as the energy content of the high-frequency storage may drift due to losses as time passes. The gray proportional feedback branch is introduced to prevent this drift. It compares the current energy content $e_p(t)$ to a reference setpoint energy content $E_{ref}$ and adjusts the power input for the peak storage accordingly. The notation will be discussed in Section III.

The filter output power $p_f(t)$ is derived from the chosen filter. The filter black box is generally implemented as a simple low-pass of first order (e.g. [7], [21], [22], [23], [29], [34], [38]), shown in Fig. 2a. It removes or drastically damps all frequencies above a cutoff frequency $f_c$. Fig. 2b illustrates the behavior of a low pass for an arbitrary signal and cutoff frequency $f_c$. This study also uses this filter type and the

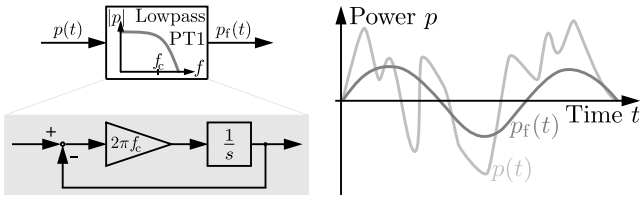


(a) Schematic layout of the first-order low-pass filter.

(b) Exemplary behavior of the implemented low-pass filter.

**FIGURE 2. Block diagram of a first-order low-pass filter (a) and the corresponding behavior (b).**

control strategy's structure in Fig. 1 as the reference. A set of equations is presented in Section III-B.

The introduced controller design, whether in the open or closed loop variant, is the most common implementation for HESS with filter-based control and can be found in many publications (e.g. [7], [9], [21], [22], [24], [25], [26], [27], [28], [29], [32], [34], [35], [38]). Other subvariants have been introduced, but the performance of these subvariants is comparable to the reference design. The assessment that these do not show superior performance or may even perform worse is supported by [9]. This study implemented four different filter-based control strategies based on literature: adaptive filter, filter combined with rule-based energy management, filter with power sharing coefficient, and filter with constant feedback. It concludes that the implemented version in this study, i.e., filter with constant feedback factor, shows the best performance, as it is the only one to adequately control the energy content $e_p$ of the peak storage to compensate losses. The study derived its results from only a single synthetic benchmark signal, and it falls short of backing up the conclusions with multiple test cases. Also, it provides no guidelines on how to design and parameterize a specific implementation. Other subvariants of filter-based control for HESS include:

### A. ADAPTIVE REFERENCE ENERGY $E_{ref}$ OR NONLINEAR FEEDBACK $k$

In this category, the reference energy $E_{ref}$ of the feedback loop, or the constant feedback factor $k$, is replaced by a more advanced set of equations or rules. In [39], a piecewise linear functional relationship is introduced that increases the constant feedback factor $k$ for higher deviations from the setpoint. A similar approach is considered in [34], which introduces a polynomial relationship instead of a constant or piecewise linear functional relationship. The authors in [26] introduce an exponential functional relationship with different exponential gains, which the authors name artificial potential field. They also introduce an adaptive reference energy $E_{ref}$ based on the energy content $e_b$ and $e_p$ of both storages.

### B. ADAPTIVE CUTOFF FREQUENCY $f_c$

This variant introduces a variable cutoff frequency $f_c$ as a function of the current energy content $e_p$ to mitigate the problem of finding the right cutoff frequency $f_c$. Further, it allows better control of the energy content $e_p$ [9]. The filter bandwidth is increased for a high energy content $e_p$ of the peak storage or decreased if the energy content is low for a positively signed input signal and vice versa for a negatively signed input signal [26], [31]. In [23], three references are introduced and compared: energy-based, voltage-based, and SOC-based reference calculation. In [30], the powers of base and peak storage are preallocated based on their energy content, and this information is used to tune the bandwidth of the low-pass filter. A fuzzy controller is used in [38] and [40] to determine the right cutoff frequency $f_c$. The former uses the input signal and energy contents $e_b$ and $e_p$ as input for the fuzzy network. The latter uses the input signal and the derivative of the input signal as input. In [41], an offline optimization is performed to find the best cutoff $f_c$ for every time step.

### C. OTHER FILTER TYPES

In this category, the first-order low pass is replaced by another filter type. All presented filter types show similar behavior. A wavelet filter is introduced in [33] and [37]. The input signal is decomposed through cascaded downsampling by a discrete haar-wavelet filter and then reconstructed by assigning the different wavelets to the different storages. In [28] and [39], a moving average filter is utilized, which smoothes the signal by calculating the mean value over a preceding time horizon of defined length. In discrete time-space, the equations for moving average and low-pass filters of the first order can be reformulated into each other [42]. A cascade of low-pass filter and slew-rate limiter is introduced in [27].

### D. COMBINATION WITH OTHER CONTROL STRATEGIES

The filter-based control is combined with other control strategies in various publications. In [29], it is overlayed by a rule-based strategy, which considers the energy contents $e_b$ and $e_p$ and driving conditions in a vehicle application. A similar approach is presented in [43], which implements a trailing fuzzy controller considering the mentioned inputs. A trailing fuzzy controller is also introduced in [44] to reduce the battery peak current. In [38], a rule-based controller complements the filter, which reacts to external event triggers in a wind farm application. In [45], a rule set is built on top of the filter that defines an energy reserve based on the energy content $e_p$ of the peak storage and reallocates low-frequency components to the peak storage to increase its utilization. An additional rule set is defined in [46] to prevent unnecessary power flow between the storages due to phase shift which leads to unnecessary losses and increased capacity. In [15], the filter-based control is complemented by an MPC to adequately set the energy reference $E_{ref}$ to increase stability and prevent system failure.

## III. MODEL AND METHODOLOGY

The first subsection introduces and discusses the used storage model and HESS model. The next one introduces the

equations for the control strategy. The following subsection outlines the simulation setup, and the last subsection defines the analyzed output characteristics.

### A. STORAGE MODEL

A storage is implemented as a unified storage model [47]. This model is technology agnostic and only characterizes a storage by high-level data sheet values: Minimum and maximum power rating $P_s^+$ and $P_s^-$, maximum energy capacity $E_s$, a linear and constant charge or discharge efficiency $\eta_s^+$ and $\eta_s^-$, where conversion losses are proportional to the current power $p_s$ and linear or constant self-discharge rate $\tau_s$, where self-discharge losses are proportional to current energy content $e_s$. Variables $e_s$ and $p_s$ are both functions of time $t$.

With these parameters, by implicitly holding the limits

$$P_s^- \leq p_s(t) \leq P_s^+ \quad \forall t \tag{1}$$

$$0 \leq e_s(t) \leq E_s \quad \forall t \tag{2}$$

the following ordinary differential equation (ODE) can be derived [47]:

$$\frac{\mathrm{d}}{\mathrm{d}t} e_s(t) = \begin{cases} \eta_s^+ \cdot p_s(t) & \text{if } p_s(t) \geq 0 \\ \frac{1}{\eta_s^-} \cdot p_s(t) & \text{if } p_s(t) < 0 \end{cases} - \frac{1}{\tau_s} e_s(t) \tag{3}$$

Note that the index "s" denotes "single storage". The equations are also valid for the indices "b" and "p", denoting "base storage" and "peak storage", which are introduced at the end of the section. The boundary conditions in Equation (1) and Equation (2) are not enforced or considered by the storage model in Equation (3) itself. The superordinate solving algorithm will ensure to fulfill these limits by adjusting the initial conditions of the ODE iteratively. Further explanation in greater detail follow in Section III-C.

There are a few advantages to justify this approach: The model is easy to parameterize for any relevant storage technology, linear, easy to implement and compute, and only takes a few parameters easily derived from datasheets. Also, it is sufficiently accurate for the high-level nature of the present study. More detailed models, which might include nonlinearities, degradation, temperature effects, or transient limitations, would not add any extra value.

Energy capacities are interpreted as net capacities, i.e., the usable amount of energy in a storage. E.g., the state of charge of a battery needs to be restricted within a specified window, which would lead to a larger gross capacity. Trailing steps need to consider this, but the usable net capacity is unaffected by this.

In this study, the storage system is not allowed to curtail the power and must completely fulfill the input power profile requirements. Both a single storage system and a HESS must be dimensioned in a way to ensure this. Mathematically, this is expressed by setting the input power profile $p(t)$ to the storage power profile $p_s(t)$ of the single storage system:

$$p(t) = p_s(t) \quad \forall t \tag{4}$$

From a system point of view, the HESS shall substitute a single storage system, and this substitution shall be transparent, i.e., the behavior of both systems shall be identical. Therefore:

$$p_s(t) = p_b(t) + p_p(t) \quad \forall t \tag{5}$$

Variable $p_b$ denotes the power of the first storage, further called base storage, and $p_p$ denotes the power of the second storage, further called peak storage. This naming convention hints at the idea that one storage shall be responsible for a steady power supply with slow variation, i.e., a base load in a broader sense. The other one shall be responsible for high power fluctuations and peaks within a power profile. Power profiles, or more generally quantities as a function of time, are furtherly called signals.

### B. CONTROL STRATEGY

Fig. 1 on page 126270 shows the structure of a filter-based HESS controller. This block diagram represents the following set of equations, including the gray feedback loop:

$$p_b(t) = p_f(t) + k(e_p(t) - E_{ref}) \tag{6}$$

$$p_p(t) = p_s(t) - p_f(t) - k(e_p(t) - E_{ref}) \tag{7}$$

Variable $k$ is the gain, and $p_f$ is the filter output power. The current energy content $e_p$ is derived from Equation (3). The reference energy content $E_{ref}$ is usually set to $E_{ref} = \frac{1}{2}E_p$ to compensate charge and discharge events [22] equally.

The first-order low-pass filter in Fig. 2a on page 126270 can be mathematically expressed as follows [42]:

$$\frac{1}{2\pi f_c} \frac{\mathrm{d}}{\mathrm{d}t} p_f(t) = p_s(t) - p_f(t) \tag{8}$$

This specific implementation is chosen because it is the most common implementation within literature (see Section II).

### C. SIMULATION SETUP

The algorithm outlined in Fig. 3 solves the previously introduced model and the underlying dimensioning problem for a specific parameter set and input signal. The used parameter values and input signals are introduced and reasoned in Section IV. The parameter set for the storage model is defined as a prerequisite, i.e., the variables $\eta_s$ and $\tau_s$. Further, the initial condition for the energy content $e_{s,0}$ arising from the first order ODE in Equation (3) must be set, and zero is arbitrarily chosen in the beginning. The energy capacity $E_s$ and rated power $P_s$ are undetermined as they are not a part of the ODE, but they will be a result at the end of the calculation (see also Section III-D). Then, the model is simulated for a chosen input signal. This step ignores the storage limits in Equation (1) and Equation (2). They will be the result at the end of the algorithm. The energy signal $e_s(t)$ will drop below zero violating the limit in Equation (2). The loop adjusts the initial condition $e_{s,0}$ by adding the offset $|\min(e_s(t))|$. This adjustment would be exact for a storage with an infinite self-discharge rate $\tau_s$. The algorithm repeats the simulation

until it converges iteratively to $\min(e_s(t)) = 0$ within a predefined precision. Then, the characteristics of interest (see following Section III-D) can be calculated from the resulting signals $p_s(t)$ and $e_s(t)$. Besides others, the needed dimension of the storage, i.e., the energy capacity $E_s$ and rated power $P_s$ are determined as a characteristic, and the limits of Equation (1) and Equation (2) will be fulfilled implicitly by this means.

Afterward, the algorithm in Fig. 3 solves the dimensioning problem for the HESS and calculates the output characteristics of base and peak storage similarly. I.e., the storage parameters for efficiency and self-discharge rate of base and peak storage $\eta_b$, $\tau_b$, $\eta_p$, and $\tau_p$ are set. Additional parameters for the control strategy, namely cutoff frequency $f_c$ and feedback factor $k$, also need to be set. Again, the initial conditions $e_{b,0}$ and $e_{p,0}$ are arbitrarily set to zero in the beginning. The system is simulated again, and the limits of Equation (1) and Equation (2) will be violated again. The initial conditions will be adjusted iteratively, repeating the simulation until both boundary conditions $\min(e_b(t)) = 0$ and $\min(e_p(t)) = 0$ are met within precision.

The output characteristics for base and peak storage defined in Section III-D are computed from the resulting signals $p_b(t)$ and $e_b(t)$ and $p_p(t)$ and $e_p(t)$. Following, they can be compared with the results of the single storage. Comparing means building a fraction of base to single and peak to single results to quantify and normalize changes.

No cyclic boundary condition is implied within the simulation and dimensioning problem, i.e., the energy content of the storage at the beginning does not equal the energy content at the end. Also, it is not implied that the storage is fully charged at the beginning and empty at the end, as the input signal may start and end with a charging event. The only boundary condition is that the storage is fully charged and discharged at least once, which the loop ensures by tuning the initial conditions.

These calculations are performed for a single parameter set for single, base, and peak storage and controller, including a single cutoff frequency $f_c$ of the low pass filter. The diagrams in the following chapters show the output characteristics, defined in Section III-D, as a function of the cutoff frequency $f_c$. An outer loop repeats the program flow depicted in Fig. 3 for a series of cutoff frequencies $f_c$. The chosen values are within a logarithmic range of $f_c \in [0.01, \ldots, 1] \cdot f_{max}$, where $f_{max}$ corresponds to the maximum occurring frequency within the frequency spectrum of the input signal. Moreover, for statistical analysis, this is repeated for a predefined set of signals. The following section introduces the input signals and setup of the numerical experiments.

### D. OUTPUT CHARACTERISTICS

The simulation results can be analyzed with respect to various output characteristics to quantify the impact of input parameter variations and to make them comparable. The analyzed characteristics include dimensions, losses, and lifetime characteristics, the latter in the form of qualitative

**Single**

set storage parameters: $\eta_s, \tau_s$
set initial condition: $e_{s,0} = 0$
**do** <solve dimensioning problem>

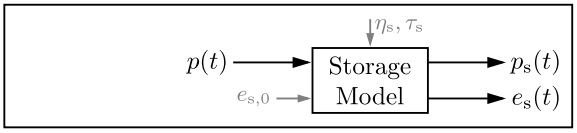


$e_{s,0} = e_{s,0} - \min(e_s(t))$
**while** $\min(e_s(t)) \neq 0$ (within precision)
$c_s = \text{compute\_characteristics}(p_s, e_s)$

**Hybrid**

set storage parameters: $\eta_b, \tau_b, \eta_p, \tau_p$
set controller parameters: $f_c, k$
set initial condition: $e_{b,0} = 0, e_{p,0} = 0$
**do** <solve dimensioning problem>

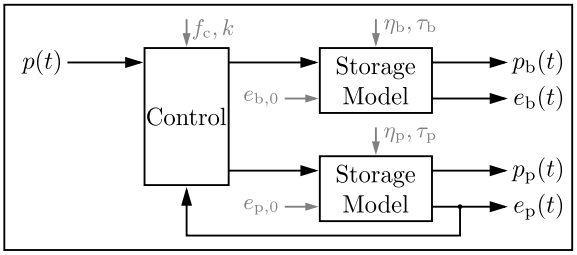


$e_{b,0} = e_{b,0} - \min(e_b(t)),\ e_{p,0} = e_{p,0} - \min(e_p(t))$
**while** $\min(e_b(t)) \neq 0 \wedge \min(e_p(t)) \neq 0$ (within precision)
$c_b = \text{compute\_characteristics}(p_b, e_b)$
$c_p = \text{compute\_characteristics}(p_p, e_p)$
$\text{compare\_results}(c_s, c_b, c_p)$

**FIGURE 3.** Pseudo code and algorithm of the simulation setup and program flow. First, the algorithm simulates the single storage with a specific parameter set and initial conditions in a loop. The loop repeats the simulation and tunes the initial conditions until the energy content boundaries are fulfilled. The same is applied to the HESS. Afterward, characteristics of Section III-D are computed and compared.

measures. The different characteristics are explained in the following.

Dimensional output characteristics include energy capacity $E$ and rated power $P$. These are easily determined with

$$E = \max(e(t)) \tag{9}$$

and

$$P = \max(|p(t)|). \tag{10}$$

Moreover, the specific power $\omega$

$$\omega = \frac{P}{E} \tag{11}$$

defined as the ratio of the two above is of interest. The specific power is a fixed value for a specific application and also fixed for most storage technologies [48]. As a result, a storage system must be overdimensioned in either power or energy to meet both requirements if the storage technology's specific power does not fit the application. A HESS combines two

storage technologies to create a system with a specific power that lies between the specific power of both technologies, which better meets the specific power of the application [48]. The specific power of a storage is similar to the C-rate of a battery but is defined more generally.

Losses are another essential characteristic. The total losses $L$

$$L = {}^{\eta}L + {}^{\tau}L \tag{12}$$

having the unit of energy can be divided into conversion losses ${}^{\eta}L$

$${}^{\eta}L = \int_0^{t_{\text{end}}} \begin{cases} p(t)(1-\eta^{+}) & \text{for } p(t) \geq 0 \\ p(t)(\dfrac{1}{\eta^{-}} - 1) & \text{for } p(t) < 0 \end{cases} \mathrm{d}t \tag{13}$$

and self-discharge losses ${}^{\tau}L$

$${}^{\tau}L = \int_0^{t_{\text{end}}} \frac{1}{\tau} e(t)\, \mathrm{d}t. \tag{14}$$

The quantification of a system's lifetime is more challenging for both specific technologies and technology agnostic approaches as performed in the present study. Therefore, two characteristics are introduced that considerably impact a storage's lifetime. The first one is the number of equivalent full cycles $C$ which is proportional to the energy throughput of a storage [47]:

$$C = \frac{1}{E} \int_0^{t_{\text{end}}} p(t) \cdot \Theta\left(p(t)\right)\, \mathrm{d}t \tag{15}$$

where $\Theta$ is the Heaviside step function. The second characteristic is the dynamic stress $S$, which is proportional to changes of a power signal, i.e., its derivative, and defined as follows:

$$S = \frac{1}{P} \int_0^{t_{\text{end}}} \left| \frac{\mathrm{d}}{\mathrm{d}t} p(t) \right| \mathrm{d}t \tag{16}$$

Both equivalent full cycles $C$ and dynamic stress $S$ are dimensionless.

Besides lifetime, it is also difficult to quantify costs in this study, as all input data and parameters are normalized or dimensionless. Furthermore, a cost model depends on a specific technology. Nevertheless, costs are addressed indirectly by the introduced output characteristics. Capital costs are primarily influenced by the dimensions of the storages, i.e., energy capacity $E$ and rated power $P$. Operational costs are primarily influenced by losses $L$, cycles $C$, and dynamic stress $S$.

## IV. REFERENCE CASE

This chapter introduces the reference case as a basis for parameter variations and studies in the next chapter. The first subsection introduces and defines the reference input signals, and the next specifies the reference model parameterization. The last one shows and explains the arising results as further studies build on these findings and representations.

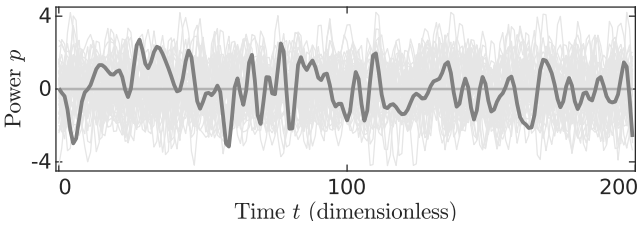


(a) Section of signals in time domain. Lighter gray: all signals superimposed. Darker gray: one randomly chosen sample.

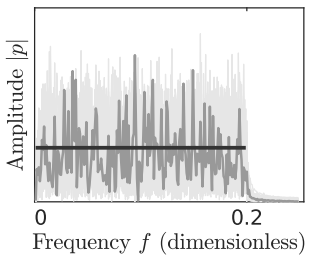


(b) Signals in frequency domain. Lighter gray: all signals superimposed; Darker gray: one randomly chosen sample; Black: averaged amplitude.

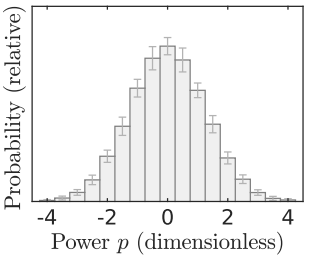


(c) Probability distribution of signal amplitudes with error bars indicating standard deviation.

**FIGURE 4. Reference input signals in time and frequency domain and probability distribution of the signals.**

### A. DEFINITION OF INPUT SIGNALS

The signal characteristics of the input signals are carefully chosen to ensure an exploitable output of the simulation studies. Moreover, to allow statistical analysis, 50 input signals were used to ensure that results are generalizable and not a statistical artifact or coincidence. The number 50 was chosen as a tradeoff between statistical validity and computational burden. The study's design leads to approximately 2000 individual simulations per signal and approximately $10^5$ simulations in total to raster all signals and parameter variations.

Fig. 4 depicts the signals. Fig. 4a shows a section of the signals and Fig. 4b shows the corresponding frequency spectra. The probability distribution of the signal values is shown in Fig. 4c. Signals are dimensionless and have 1000 sampling points. It is up to the reader to interpret the sampling rate in seconds, minutes, quarter hours, or anything else. The signals are generated with a random Gaussian white noise filtered by a linear phase finite impulse response (FIR) lowpass with a steep cutoff at 1/5 of the sampling rate. I.e., if the sampling rate is interpreted as 1 s, the signal is a limited white noise with 0.2 Hz cutoff.

The generated signals were scaled and transformed to enforce a mean value of 0 and a rectified value of 1. With this normalization, the root mean square value, maximum value, and derived signal characteristics as form or crest factor of the signals would still reveal a Gaussian distribution. The 50 input signals were filtered and selected out of $10^5$ generated signals. Those signals with identical (within precision) root mean square and maximum value at the peak of the Gaussian distribution were selected to normalize

**TABLE 1. Characteristics of input signals used to perform simulation.**

| | | |
|---|---|---|
| Number of signals | N | 50 |
| Sampling points | n | 1000 |
| Freqency spectrum | | bandlimited white noise (cp. Fig. 4b) |
| Mean value | $\frac{1}{T}\int_0^T p(t)\,\mathrm{d}t$ | 0 |
| Rectified value | $\frac{1}{T}\int_0^T \lvert p(t)\rvert\,\mathrm{d}t$ | 1 |
| Root mean square | $\frac{1}{T}\sqrt{\int_0^T p^2(t)\,\mathrm{d}t}$ | $1.252^{+0.009}_{-0.003}$ (abs. deviation) |
| Max. abs. value | $\max(\lvert p(t)\rvert)$ | $4.2 \pm 0.013$ (abs. deviation) |

these signal characteristics. This measure asserts that the characteristics of all signals are (nearly) equal and do not show variance anymore. It ensures that statistical deviations shown in the output are not a consequence of statistical deviations of the input propagated through the simulation. The root mean square value is 1.252 and the maximum value is 4.2. Table 1 summarizes the properties of the signals.

### B. MODEL PARAMETERS

For simplicity, power ratings $P_\mathrm{s}^+$ and $P_\mathrm{s}^-$ are symmetrically set to the same absolute value, leading to an identical charge and discharge power:

$$\begin{aligned} P_\mathrm{s}^+ &= P_\mathrm{s} \\ -P_\mathrm{s}^- &= P_\mathrm{s} \end{aligned} \tag{17}$$

The same is applied to charge and discharge efficiency:

$$\begin{aligned} \eta_\mathrm{s}^+ &= \eta \\ \eta_\mathrm{s}^- &= \eta \end{aligned} \tag{18}$$

The efficiency of the storage is set to $\eta = 0.95$. This value is more or less arbitrarily chosen, but many electrical energy storages fall into the magnitude of this parameter. The self-discharge rate $\tau$ is only meaningful in conjunction with the simulation time. It is set at a value that self-discharge losses ${}^{\tau}L$ and conversion losses ${}^{\eta}L$ are in a comparable magnitude. Moreover, it is determined for each signal individually to ensure that the total losses $L$ that result for each signal are equal:

$${}^{\eta}L + {}^{\tau}L = \text{const.} \quad \forall \text{ signals} \quad \text{(within precision)} \tag{19}$$

The total losses where set to ${}^{\eta}L + {}^{\tau}L = 100$[1] and each individual loss component has an approximate share of 50.

The individual self-discharge rate $\tau_\mathrm{s}$ is determined similarly to the algorithm shown in Fig. 3. The storage ODE is forward simulated, and the initial condition is adapted until the boundary condition is met. Besides the initial conditions, the algorithm adapts the self-discharge rate $\tau_\mathrm{s}$ and checks if the losses $L$ meet the criteria in Equation (19). This leads to self-discharge rates of $\tau_\mathrm{s} = 1084 \pm 213$[2] (std. deviation).

The feedback factor $k$ is set to $k = 0.01$. This value is empirically determined in prestudies and found to be an adequate choice for the reference case. The parameterization is summarized in Table 2.

[1]No units, has the dimension of energy.
[2]No units, has the dimension of time.

**TABLE 2. Reference storage and control model parameters.**

| | | |
|---|---|---|
| Efficiency | $\eta$ | 0.95 |
| Self discharge rate* | $\tau$ | $1084 \pm 213$ (std. deviation) |
| Control strategy | | Low pass with feedback loop |
| Feedback factor | $k$ | 0.01 |

*$\eta$ and $\tau$ are chosen in a way that ${}^{\eta}L \approx {}^{\tau}L$. Moreover, $\tau$ is set for each signal individually to ensure that ${}^{\eta}L + {}^{\tau}L = \text{const.}\ \forall$ signals.

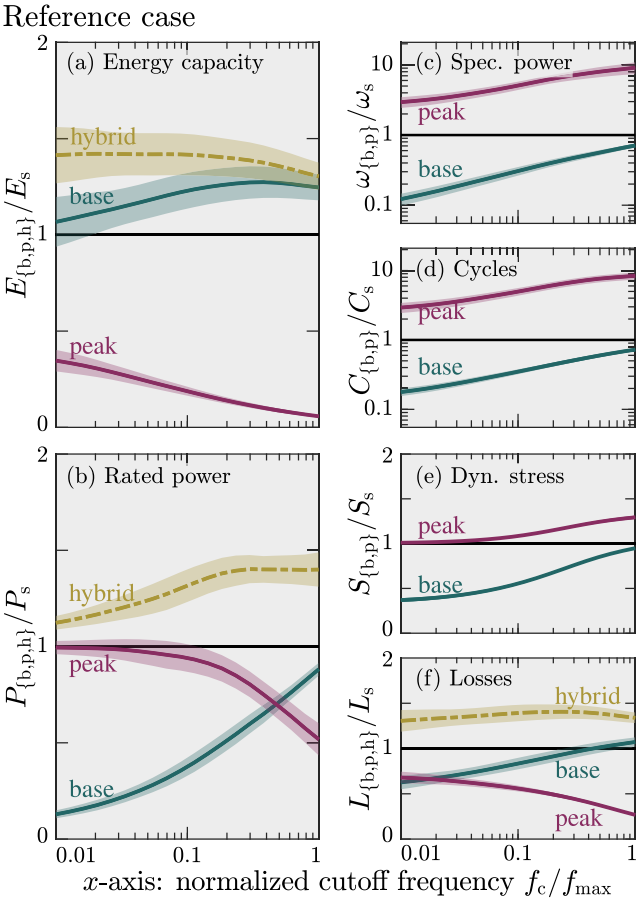


**FIGURE 5. Results of the reference case utilizing Table 1 and Table 2 as input and parameter definition. Output characteristics for base, peak, and added hybrid storage shown as a function of the cutoff frequency of the lowpass. All characteristics are normed with respect to the value of the corresponding single storage with ideal dimensions. Shaded areas indicate standard deviation (equal to error bars). It can be seen that overall dimensions (a) and (b) and losses (f) increase but specific power (c), cycles (d), and dynamic stress (e) change beneficially.**

The free parameter subject to variation is the filter cutoff frequency $f_\mathrm{c}$, and the output characteristics defined in Section III-D are a function of this cutoff frequency $f_\mathrm{c}$. Changes to reference parameters are the subject of investigation in further parameter studies in the next chapter. Before, the following section discusses the reference case.

### C. SIMULATION RESULTS

Fig. 5 shows the simulation results for the reference case defined in the previous sections. The figure consists of six subfigures (a–f); each shows one output characteristic defined in Section III-D. Fig. 5a and Fig. 5b on the left side show the results for energy capacity $E$ and rated power $P$,

whereas Fig. 5c to Fig. 5f on the right side show the output characteristics for specific power $\omega$, equivalent full cycles $C$, dynamic stress $S$ and losses $L$. The $x$-axis of all subfigures depicts the cutoff frequency $f_c$ of the filter normalized by the maximum occurring frequency $f_{max}$ in the frequency spectrum of the input signal ($0.2 \cdot f_{sample}$). The $x$-axis is logarithmic, ranging two decades from 0.01, i.e., 1 % of the maximum occurring frequency to 1, i.e., the filter cutoff frequency $f_c$ coincides with maximum occurring frequency $f_{max}$ of the signal.

The output characteristics on the $y-$axes of base storage, peak storage, and hybrid storage (sum of the former two) are normalized by the corresponding value of the single storage to show relative changes of these with reference to the single storage. I.e., they are divided by the output characteristic values of the single storage. Therefore, each diagram has a horizontal black line at a value of one to visualize the reference to the single storage. All subfigures show a normalized output characteristic of base storage (turquoise), peak storage (violet), and hybrid storage (if reasonable, dashed ocher) as a function of the normalized cutoff frequency $f_c$ of the filter. As each diagram is generated by the results of 50 input signals, each line represents the mean value of the results, and the shaded semitransparent areas represent the standard deviation. For enhanced visual clarity, this representation was chosen instead of error bars. A Gaussian normal distribution adequately approximates the distribution. I.e., mean and median values are almost identical, and the distribution does not show significant skewness or excess kurtosis.

It can be seen in Fig. 5a that the total energy capacity $E_h$ of the hybrid storage system is larger than that of the single storage reference $E_s$ by 30 % to 50 %. This effect is relatively independent of filter cutoff frequency $f_c$, although the values for peak and base storage change with varying cutoff frequency $f_c$. I.e., the sum of the energy capacities $E_b$ and $E_p$ of base and peak storage is roughly constant. The energy capacity $E_b$ of the base storage alone is larger than the capacity $E_s$ of the single storage by 5 % to 30 %. On the other hand, the peak storage energy capacity $E_p$ is only a fraction, i.e., 5 % to 40 %, of the single storage energy capacity $E_s$. The increased capacity $E_h$ of the hybrid storage system arises through additional losses $L$ due to power or energy exchange between base storage and peak storage, which are nonexistent in a single storage system. There is a slight tendency of larger peak storages $E_p$ and smaller base storages $E_b$ towards low filter cutoff frequencies $f_c$, which is plausible as lower cutoff freqencies $f_c$ lead to higher shares of the input signal for the peak storage.

The effects on the rated power $P_b$ and $P_p$ of base and peak storage are the other way around (cp. Fig. 5b). While the rated power $P_b$ of the base storage is drastically reduced with low cutoff frequencies $f_c$ and tends towards 0, the rated power $P_p$ of the peak storage tends towards 1, i.e., the rated power $P_s$ of the single storage. The total rated power $P_h$ of the hybrid storage system is again larger than that of the single storage system by 10 % to 50 %, but the overdimensioning in power diminishes with low cutoff frequencies $f_c$.

As a consequence of the relations shown in Fig. 5a and Fig. 5b, the specific powers $\omega_b$ and $\omega_p$ of the storages show a large deviation from the original single storage's specific power $\omega_s$ by a factor of 2 to 10 each (cp. Fig. 5c). For high cutoff frequencies $f_c$, the base storage's specific power $\omega_b$ tends towards 1, while the peak storage's specific power $\omega_p$ tends towards 10. For low cutoff frequencies $f_c$, the base storage tends towards 0 while the peak storage tends towards 1, which means that the hybrid storage system degenerates to the properties of the single storage system.

The feature of differing specific powers $\omega$ can be exploited beneficially as the specific power of the application typically does not match the specific power of any storage technology. Then, the specific power of the application can be represented by two storages with varying specific power. This feature mitigates the overdimensioning effect in Fig. 5a and Fig. 5b to a certain extent because a single storage technology has to be overdimensioned in either power $P$ or energy $E$ to meet the requirement of the other one.

In Fig. 5d and Fig. 5e, it can be seen that cycles $C_b$ and dynamic stress $S$ are drastically reduced for the base storage, especially for lower cutoff frequencies $f_c$, at the cost of increased cycles $C_p$ and stress $S_p$ for the peak storage. The effect on cycles $C$ is approximately proportional to those on specific power $\omega$. On a linear scale, this is also true for dynamic stress $S$. The reduced cycles $C_b$ and stress $S_b$ of the base storage translate antiproportionally into substantially increased lifetime, while the peak storage presumably can cope well with the increased cycles $C_p$ and stress $S_p$. This effect is reasonable and expectable, as this is the primary intention of the investigated filter-based control strategy.

The effect on the losses $L$ in Fig. 5f correlates with the relationships for the energy capacity $E$ in Fig. 5a. The total losses $L_h$ of the HESS increase by 30 % to 50 % compared to the losses $L_s$ of a single storage system, independently from the chosen cutoff frequency $f_c$. I.e., the sum of the losses $L_b$ and $L_p$ of base and peak storage is roughly constant, although the values for peak and base storage change with varying cutoff frequency $f_c$. The losses $L_p$ of the peak storage increase towards lower cutoff frequencies $f_c$ proportionally to the increase in energy capacity $E_p$ (cp. Fig. 5a). It is the other way around for the base storage.

The standard deviations of all results are between 10 % to 15 %. The bootstrapped 95 % confidence intervals for the mean value are between 1 % to 5 % and between 15 % to 25 % for the standard deviation. These quantities are also present within the subsequent parameter variations. On the one hand, the standard deviation is high enough to be accounted for while dimensioning a storage system for a real problem because the dimensioning process reveals uncertainty to some extent. On the other hand, the deviation is small enough to justify the generalization of the results and findings, as the results are qualitatively equal for each input signal.

**TABLE 3. Parameter variations and studies for input signal, storage, and control model.**

| Section | Ref. Value | Variations | |
|---|---|---|---|
| V-A Freq. Spectrum | equal<br>cp. Fig. 4b | low<br>cp. Fig. 6a | high<br>cp. Fig. 6b |
| V-B Mean value | 0 | -0.1 | -0.2 |
| V-C Loss model | $\eta = 0.95$ *1 | $\eta_\mathrm{b} = 0.93$ *2<br>$\eta_\mathrm{p} = 0.97$ | $\eta_\mathrm{b} = 0.91$ *3<br>$\eta_\mathrm{p} = 0.99$ |
| V-D Feedback $k$ | 0.01 | 0.001 | 0 |

*1 $\tau = 1084 \pm 213$
*2 $\tau_\mathrm{b} = 1853 \pm 359,\ \tau_\mathrm{p} = 758 \pm 158$
*3 $\tau_\mathrm{b} = 5774 \pm 1020,\ \tau_\mathrm{p} = 570 \pm 121$

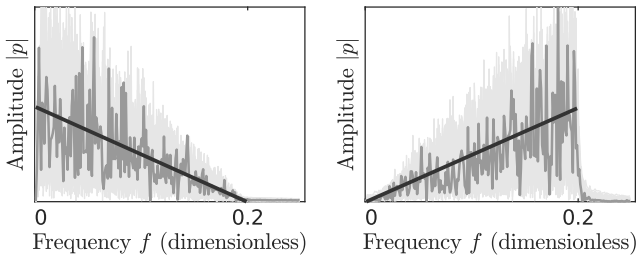


(a) Frequency spectrum of low-frequency signals

(b) Frequency spectrum of high-frequency signals

**FIGURE 6. Variation of the frequency spectrum of the input signals to study the effect on the output characteristics (cp. Fig. 4b and Fig. 7).**

At last, it shall be stated that the results for the increased dimensions $E$ and $P$ (cp. Fig. 5a and Fig. 5b) and losses $L$ (cp. Fig. 5f) fundamentally contradict the results stated in [48]. This paper performs an analytic derivation, proving that a single storage can always be split into two hybrid storages with the same total energy capacity $E$ and total rated power $P$, respecting the boundary condition of optimal control. It can be deduced that a filter-based control paradigm is not optimal from a dimensional viewpoint. It also contradicts the results of papers that show smaller dimensioning for filter-controlled HESS (e.g. [24], [36]). The reduced dimensions come from the fact that these papers do not have an ideal single storage as a reference but an arbitrary specific storage technology. Also, nonlinear loss models alter the results, e.g., quadratic loss models as in [49]. On the other hand, the results in this study are backed up by [21], which also observes increased dimensions $E$ and $P$ for filter-controlled HESS.

The presented results are only obtained by numerical simulations and are not backed up by a physical experimental setup. Nevertheless, numerous publications are presenting experimental validation for filter-controlled HESS (e.g. [23], [27], [28], [39], [40], [43], [46]), attesting a high consistency between numerical and experimental data. I.e., it can be assumed with a high degree of confidence that the results obtained in this study also hold in a real-world experimental setup.

## V. PARAMETER VARIATIONS

The following parameter studies are based on the reference case presented in the previous section. The effects of the parameter variations are displayed in the same style and described accordingly in the next subsections. The present work presents four parameter studies in three categories which are summarized in Table 3. Each row of lists provides information about one parameter variation. The first column ''Section'' provides a name for this variation and refers to the section within the paper describing it in detail. The second column ''Ref. value'' repeats the reference value of the varied parameter. The reasoning for the reference values is provided in Section IV-A and Section IV-B. The third and fourth columns ''Variations'' list the modification of the reference value in the parameter variation. The values of these varied parameters are empirically determined to produce meaningful results and figures. I.e., the parameters' magnitude and range are set so that the results significantly change.

Firstly, the influence of the frequency spectrum is analyzed. The white noise with an equally weighted distribution of frequencies is filtered in a way to either emphasize lower frequency parts or higher frequency parts. The next signal variation analyses the influence of the mean value of the input signals by introducing an offset along the $y$-axis. The next variation relates to the storage model parameters efficiency $\eta$ and self-discharge rate $\tau$. It equips the base storage with a better self-discharge rate but a worse efficiency and the peak storage with a better efficiency but a worse self-discharge rate. At last, the feedback factor $k$ of the control loop is varied and analyzed. The individual sections provide further information for each parameter variation. In the present work's context, further studies and parameter variations have been performed that did not show significant insights. Therefore, they are not discussed in detail and are only listed at the end of the section. If the reader is only interested in the results and derived conclusions, it is possible to skip the detailed descriptions within this section or only view the results in Fig. 7 to Fig. 10 and continue with Section VI on page 126281.

### A. VARIATION OF FREQUENCY SPECTRUM OF INPUT SIGNAL

The original input signals are filtered via a FIR filter that skews the input signals' original equally-weighted frequency spectra towards low or high frequencies. The resulting frequency spectra are depicted in Fig. 6. In Fig. 7, the previously introduced results of the reference case (cp. Fig. 5) are complemented by the results arising from variation of the frequency spectrum. The color coding is retained, the results of the signals with weight on the low-frequency components (cp. Fig. 6a) are in brighter shades, and the signals with weight on the high-frequency components (cp. Fig. 6b) are depicted in darker shades. Additionally, gray arrows indicate the change from low- to high-frequency signals. Apart from the different frequency spectra, all other signal characteristics shown in Table 1 remain unchanged.

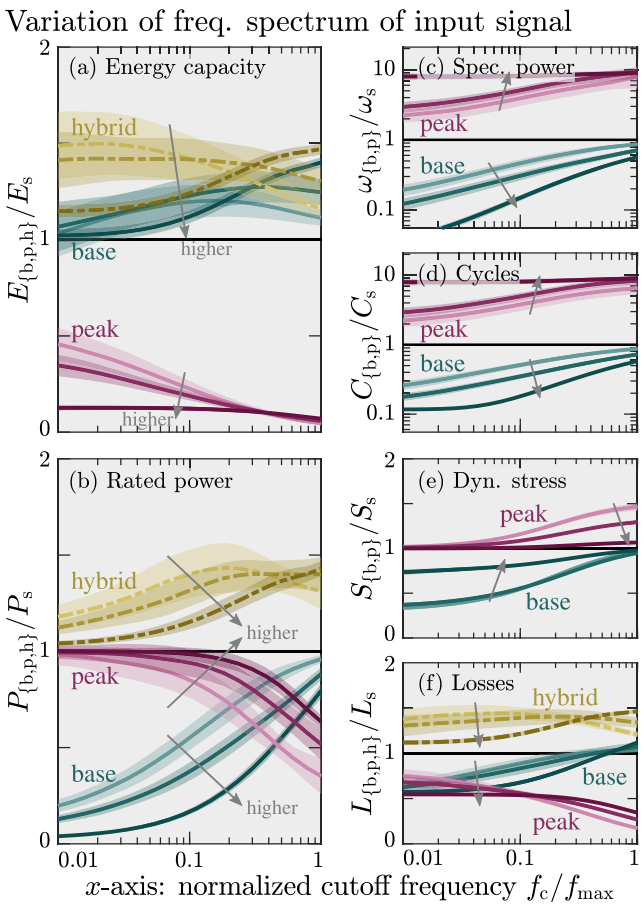


**FIGURE 7.** Changes in the results by varying the frequency spectrum of the input signal (cp. Fig. 6). Representation of results equivalent to Fig. 5. Darker coloring from low- to high-frequency spectrum of the input signals, additionally indicated by gray arrows. For low cutoff frequencies $f_c$, high-frequency input signals lead to higher spreads in specific power (c), reduced cycles for base storage (d), and smaller total dimensioning (a), (b).

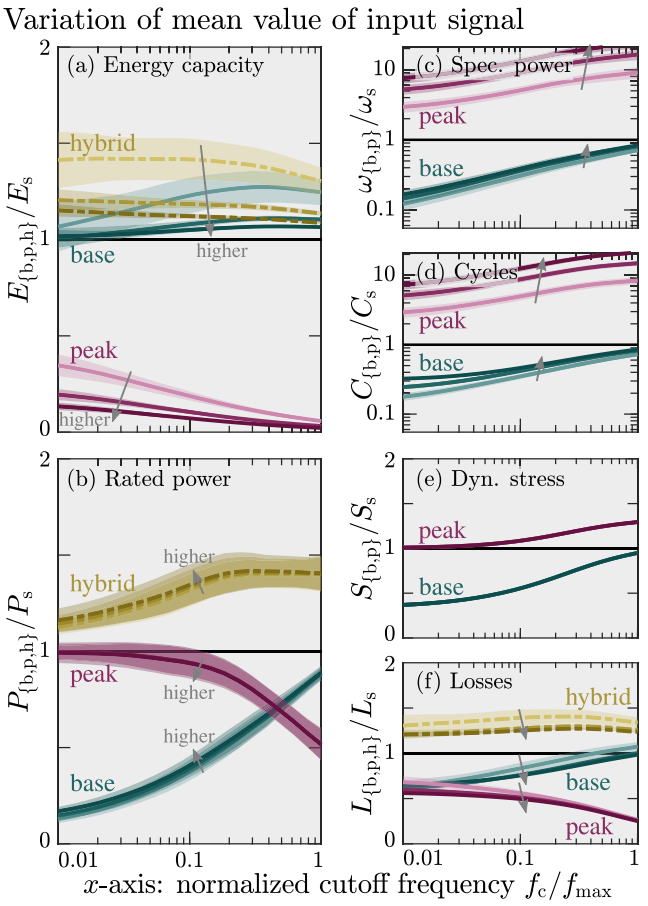


**FIGURE 8.** Changes in the results by varying the mean value of the input signal from 0 to −0.1 to −0.2. Representation of results equivalent to Fig. 5. Darker coloring indicates a higher deviation from zero of the mean value of the input signal, additionally indicated by gray arrows. With higher deviation, base and hybrid energy capacity (a) tend towards single storage dimensioning. Power rating (b) is virtually unaffected. High increase of specific power (c) and cycles (d) for peak storage. Nonetheless, hybridization is less reasonable for high mean value signals as base storage results tend towards single storage results.

In Fig. 7a, it can be seen that the peak storage energy capacity $E_p$ gets smaller for input signals with pronounced high-frequency parts, especially if low cutoff frequencies $f_c$ are chosen for the controller. Results for base storage and combined HESS are mixed throughout the $x$-axis. The spread of the rated power $P$ (Fig. 7b) gets more pronounced for input signals with pronounced high-frequency parts. The overall losses are reduced for the hybrid system for signals with pronounced high-frequency parts.

The spread of the specific powers $\omega$ becomes more distinct for higher frequency signals as well as the spread in full cycles $C$ (Fig. 7c and 7d). On the other hand, the dynamic stress $S$ of both storages converges to the original single storage and becomes less distinct (Fig. 7e). The absolute dynamic stress $S$ increases for all storages. However, as the single storage system's value normalizes the results, the curves tend toward the single storage. The effect on losses $L$ is mixed, but losses $L$ are generally lower for lower cutoff frequencies $f_c$.

In summary, high-frequency-weighted signals offer more potential for design (higher spread in specific power $\omega$) and stronger cycle reduction $C_b$ for the base storage and provide higher diversion between the base and peak storage characteristics.

### B. VARIATION OF MEAN VALUE OF INPUT SIGNAL

Next, the influence of the mean value of the input signal is investigated. The original input signals are defined with a mean value of zero. The introduced variation shifts the signals along the $y$-axis by $-0.1$ and $-0.2$ (cp. Table 3) with a simple subtraction. With this, the signal parameters in Table 1 inevitably change, but the frequency spectrum in Fig. 4b is reserved. Subtraction leads to a more pronounced discharging phase with fewer intermediate charging spikes.

The mean value parameter variation results are shown in Fig. 8. Darker shading indicates a higher deviation of the mean value from zero. The brightest color set shows the reference case with a mean value of zero, while the darkest color set shows the results for a mean value of $-0.2$.

The peak storage capacity $E_p$ tends towards zero, and the base storage capacity $E_b$ towards one for input signals with higher mean value offset. Hence, the hybrid system energy capacity $E_h$ also tends towards one (cp. Fig. 8a). The reason is that the absolute peak storage energy capacity $E_p$ is unaffected by the mean value of the signal, but the absolute base storage energy capacity $E_b$ increases. The normalization with the single storage energy capacity $E_s$ (which also gets larger) leads to an equalization.

For the chosen mean value variations, the effect on the rated power $P$ is negligible, as the normalization with the single storage cancels the changes (cp. Fig. 8b). For higher mean value offsets, the power rating of the base storage $P_b$ would tend towards one, and the peak storage energy capacity $P_p$ would tend towards zero because the input signals will degenerate to a constant signal with vanishingly small noise.

With higher mean value offsets, the specific power $\omega_p$ of the peak storage substantially increases compared to the single storage $\omega_s$, which is again an effect of normalization (cp. Fig. 8c). It stays essentially unaffected in absolute values. There is only a slight effect on the normalized specific power $\omega_b$ of the base storage, which tends toward one. The same effects can be seen for the number of cycles $C$ (cp. Fig. 8d).

The dynamic stress $S$ (cp. Fig. 8e) is unaffected by an offset of the mean value, as it vanishes through the derivative in Equation (16). The overall losses $L_h$ decrease and tend towards the single storage losses $L_s$ as the relative proportion of power flow between storages decreases (cp. Fig. 8f).

The mean value of the signal has a significant impact on the results. While it may seem that a high mean value is a good indicator of the effective utilization of a HESS, the opposite is true. Although total dimensions $E_h$ and total losses$L_h$ decrease and the differences in specific powers $\omega$ increase, the positive gains for the base storage compared to the single storage vanish. At a certain point, the dynamic part of the input signal becomes negligible compared to the stationary part, and the peak storage only removes the ripple, which does not seriously impact the base or single storage.

### C. VARIATION OF LOSS MODEL OF STORAGE MODEL

This section investigates the influence of the self-discharge rate $\tau$ and efficiency $\eta$ on the results. The parameterization of the reference case is $\eta = 0.95$ and $\tau = 1084 \pm 213$ for both peak and base storage (cp. Table 3). Now, the parameters are varied: The base storage efficiency and the self-discharge rate are decreased, leading to higher conversion but lower self-discharge losses. The peak storage efficiency and the self-discharge rate are increased, leading to lower conversion but higher self-discharge losses. However, the total losses $L$ stay equal, i.e., ${}^{\eta}L + {}^{\tau}L = \text{const.}$, i.e., each storage would produce the same total losses as the original single storage if used on its own.

The modified pairings are

- $\eta_b = 0.93$, $\tau_b = (1853 \pm 359)$,
  $\eta_p = 0.97$, $\tau_p = (758 \pm 158)$ and

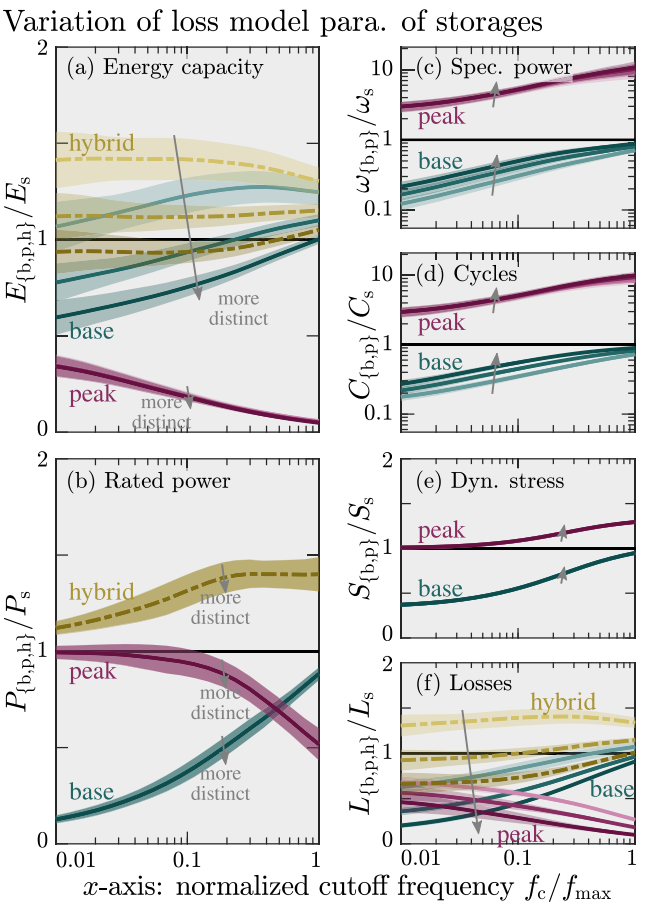


**FIGURE 9.** Changes in the results by varying the loss model parameterization of the storage model (cp. Fig. 6). Representation of results equivalent to Fig. 5. Darker coloring implies increased efficiency and self-discharge rate variation between base and peak storage. Distinct loss models can lead to smaller total hybrid energy capacity (a) and reduced losses (f) by simultaneously reducing cycles (c) and stress (d) for the base storage. Power rating (b) is virtually unaffected.

- $\eta_b = 0.91$, $\tau_b = (5774 \pm 1020)$,
  $\eta_p = 0.99$, $\tau_p = (570 \pm 121)$.

The results of the loss model parameter are displayed in Fig. 9. Darker color sets indicate more distinct loss models, while the brightest color set displays the reference case where base and peak storage have the same loss model parameters $\eta$ and $\tau$.

The varying parameterization of the loss models introduces a double benefit. The increased efficiency $\eta_p$ of the peak storage reduces the conversion losses ${}^{\eta}L$ of fast charging and discharging events as the peak storage is exposed to the high-frequency components. As it only needs a small energy capacity $E_p$ to handle these events, the poorer self-discharge rate $\tau_p$ is negligible. It is the other way around for the base storage: A worse efficiency $\eta_b$ is more tolerable, as the storage is not exposed to rapid charge and discharge events due to the low-frequency parts assigned by the controller. On the other hand, the better self-discharge rate $\tau_b$ leads to lower losses for the high energy amounts $E_b$ that the base storage has to reserve.

This benefit is prominently supported by Fig. 9f: Losses for both base $L_b$, peak $L_p$ and hybrid storage $L_h$ significantly decrease with a more distinct loss model parameterization. At a certain point, the total losses $L_h$ fall below the original single storage reference $L_s$. Fig. 9a also reflects decreased overall losses, which shows the energy capacities $E$. While the peak storage energy capacity $E_p$ is unaffected, the needed base storage energy capacity $E_b$ is significantly reduced with a more distinct loss model parameterization. Again, at a certain point, the energy capacity $E_h$ of the hybrid storage falls below the energy capacity $E_s$ of the single storage system.

There is no change in rated power $P$, as it is unaffected by the efficiency $\eta$ and self-discharge rate $\tau$ (cp. Fig. 9b). The same applies to the dynamic stress $S$ (cp. Fig. 9e). The specific power $\omega_b$ of the base storage (Fig. 9c) increases because the energy content $E_b$ decreases. The specific power $\omega_p$ for the peak storage is unaffected by changes in the loss model parameterization. The cycles $C$ of the base storage (Fig. 9d) increase relative to the single storage $C_s$ as the energy throughput in absolute numbers is roughly the same for all loss model parameterizations. However, the energy content reference $E$ in the denominator decreases.

In summary, a filter-controlled HESS that utilizes storages with distinct loss model parameterization optimally takes advantage of the traits of each storage, which can even lead to smaller energy capacities $E_h$ and lower losses $L_h$ than the original single storage reference $E_s$ and $L_s$.

### D. VARIATION OF k FEEDBACK FACTOR OF CONTROL

At last, the variation of the feedback factor $k$ is investigated. The feedback loop is a proportional control instance for the energy content $e_p$ of the peak storage, as described in Section III and Fig. 1. If the energy content $e_p$ of the peak storage deviates from a set point $E_{ref}$, which is half of its energy content $E_p$, the feedback loop counters these changes. Higher feedback factors $k$ lead to a more aggressive compensation that diminishes the effect of the leading low-pass filter. The main effect of the feedback loop is retained with a reasonably tuned feedback factor $k$: It compensates conversion and self-discharge losses ${}^{\eta}L_p$ and ${}^{\tau}L_p$ of the peak storage, which leads to smaller energy capacities without introducing high-frequency power demands for the base storage.

The reference value of the feedback factor is $k = 0.01$, the investigated parameter changes are $k = 0.001$ and $k = 0$, i.e. no feedback or open loop control (cp. Table 3). Fig. 10 shows the results of the feedback factor $k$ variation. Darker coloring/shading indicates higher feedback factor $k$, i.e., more aggressive leveling, while brighter colors indicate a gentler set point correction. The brightest color set encodes the open loop control $k = 0$ while the darkest color set encodes the reference case $k = 0.1$.

Higher feedback factors $k$ lead to much smaller energy capacities $E_p$ of the peak storage at the cost of higher base storage dimensioning $E_b$ and overall dimensioning $E_h$

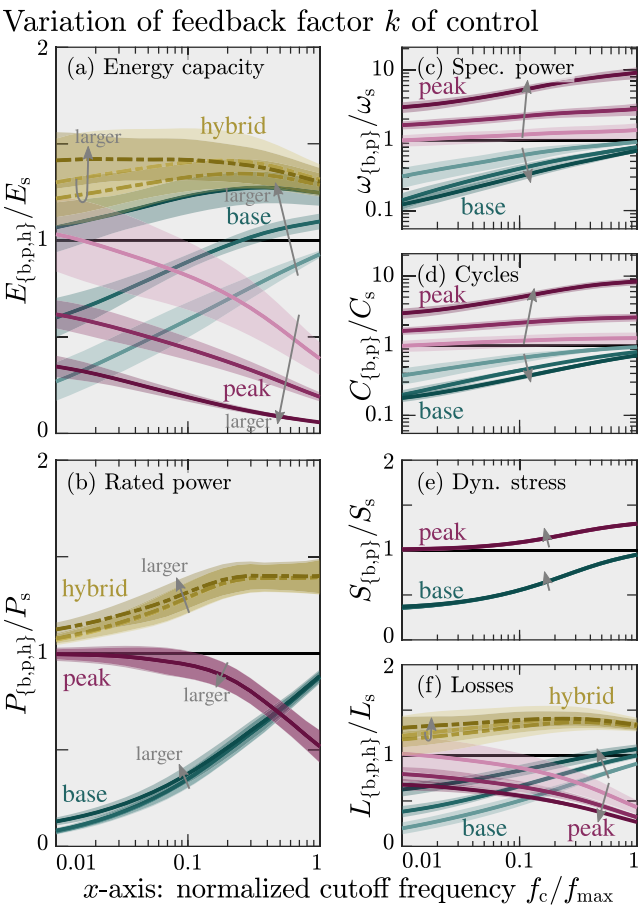


**FIGURE 10.** Changes in the results when varying the feedback factor $k$ of the control strategy. Representation of results equivalent to Fig. 5. Darker coloring implies larger $k$ factor (from 0 to 0.001 to 0.01.) Larger $k$ factors lead to smaller peak energy capacity (a) and higher specific power (c) at the cost of higher overall energy capacity (a) and losses (f).

(cp. Fig. 10a). The total energy capacity $E_h$ of the hybrid system stays roughly the same. The same applies to the losses $L$, as seen in Fig. 10f.

The feedback factor $k$ does not significantly influence the rated power $P$ (cp. Fig. 10b). Following, the spread in specific power $\omega$ (Fig. 10c) between base and peak storage increases with increasing feedback factor $k$. The influence of the feedback factor $k$ on the specific power can be exploited: By tuning the feedback factor $k$ the designer can choose a pairing of specific powers $[\omega_b, \omega_p]$ for base and peak storage that matches existing storage technologies.

The cycles $C_p$ of the peak storage rise with increasing feedback factor $k$ (cp. Fig. 10a) because the energy capacity $E_p$ decreases, while the absolute amount of energy throughput is roughly constant. It is the other way around for the base storage cycles $C_b$. The dynamic stress $S$ shown in Fig. 10e is nearly unaffected by the feedback factor $k$, as the feedback loop mainly compensates losses without altering the input signals of the storages significantly.

In summary, the feedback factor $k$ does not significantly influence the total dimensions $E_h$ and $P_h$ and losses $L_h$ of the hybrid system. However, a significant influence on the

dimensions $E_b$ and $E_p$ of the individual peak and base storage makes it a crucial design variable.

Special notes concerning open loop control ($k = 0$): The energy capacities $E_b$ and $E_p$ of the open loop filter tend toward zero and one at the edges of the normalized cutoff frequency axis $f_c$. This alignment is reasonable as the controller assigns the complete signal to one storage alone without feedback. Nevertheless, it will not reach precisely zero, as the filter introduces a phase shift between filter output and input. The rated powers $P_b$ and $P_p$ weakly correlate to the energy capacities $E_b$ and $E_p$. As a result, the spread in specific power $\omega$ is comparably indistinctive to control strategies with feedback. Also, the cycle reduction $C_b$ for the base storage is relatively small compared to the closed-loop control ($k \neq 0$), and all results are subject to an increased standard deviation, which needs to be considered with higher safety margins for dimensioning. It can be deduced that the effectiveness of the open loop control is poor.

### E. ADDITIONAL STUDIES

Other investigations were performed in the context of the present study, but the presentation of the results is omitted to increase significance and conciseness. Nevertheless, this section provides a short discussion on the omitted results.

#### 1) OTHER TYPES OF FILTERS

Other filter types were investigated, among them higher order filters, highpass filters, FIR filters, and infinite impulse response (IIR) filters. They all expose the same behavior, and the choice is insignificant, except for high-order filters. Due to the high phase shifts introduced by these filters, the power allocation is poor, which leads to inferior performance.

#### 2) RAMP FILTER

A ramp filter does not limit a frequency $f$ but limits the maximum allowed slope, i.e., the allowed change in power per time or its derivative $\mathrm{d}p/\mathrm{d}t$. This implementation is more typical for power electronics than for a low-pass filter or a restriction for applications such as wind power smoothing [50]. The qualitative results are comparable if the maximum slope $\mathrm{d}p/\mathrm{d}t$ and cutoff frequency $f_c$ at the $x$-axis are scaled correctly. However, the results for the ramp filter are subject to an increased standard deviation, which needs to be accounted for with higher safety margins during dimensioning.

#### 3) VARIATION OF REFERENCE LOSS MODEL PARAMETERIZATION

Other values for the efficency $\eta$ and self-discharge rate $\tau$ that are equally applied to the single, base, and peak storage, do not alter the normalized results. Changes only happen if they are applied unequally between the base and peak storage, as described in Section V-C.

#### 4) DYNAMIC STRESS

The dynamic stress $S$ introduced in Equation (16) is an abstract measure of the variation of a signal with the claim that lifetime correlates with it. Other definitions were tested, among them the examination of the maximum slopes or the investigation of the power density spectrum at low and high frequencies, but all showed qualitatively comparable results. The present one is chosen because it is simple and symmetric to the definition of the cycles in Equation (15).

#### 5) LENGTH OF SIGNAL

The length $N$ of the signal will affect the energy capacity $E_b$ of the base storage, but not the energy capacity $E_p$ of the peak storage. The absolute energy capacity $E_b$ of the base storage increases with increasing signal length $N$, and the absolute amount of the peak storage energy capacity $E_p$ stays constant. Through normalization, the curves will tend towards one and zero, respectively. The rated power $P$ stays unaffected for both storages. As a result, the normalized specific powers $\omega_b$ and $\omega_p$ will tend towards one for the base storage and towards infinity for the peak storage. Cycles $C$ will behave the same way. The normalized dynamic stress $S$ is unaffected by signal length $N$. Also, the length of the signal $N$ does not impact the losses $L$. This is an implicit consequence of the simulation setup definition, as the loss model parameters $\eta$ and $\tau$ are chosen to have equal weight on efficiency and discharge losses ${}^{\eta}L$ and ${}^{\tau}L$.

#### 6) SIGNAL GENERATION

Other kinds of signal definition, e.g., a univariate random generator instead of a Gaussian random generator or other shapes of the frequency spectrum, were analyzed. However, the results did not reveal any differing or extra insights.

#### 7) SUPERPOSITION

The qualitative results presented in the previous sections can be superposed. E.g., it is shown in Section V-A that high-frequency signals lead to higher specific powers $\omega_p$ of the peak storage, and in Section V-B it is shown that higher deviation from the mean value of the signal also leads to higher specific powers $\omega_p$ for the peak storage. Combining both effects would increase the specific power $\omega_p$ even further.

## VI. KEY FINDINGS AND DESIGN GUIDE

The following section gathers insights of the previous elaborations. The methodology can be used as a dimensioning tool, but the idea is to present dependencies, correlations, influences, and advice in a condensed form. They can be kept in mind and incorporated into individual design processes. First, key findings are extracted, and then design guidelines are derived from these.

### A. KEY FINDINGS

The following conclusions are rules of thumb extracted from the previous elaborations. The designer can always look up details in the individual sections.

1)
A filter-controlled HESS benefits from an increased lifetime (in terms of cycles $C_b$ and dynamic stress $S_b$) of the base storage at the cost of higher energy capacity $E_h$ and rated power $P_h$ of the hybrid system compared to the single storage system (cp. Section IV-C). Hence, the filter control performs worse than other control strategies regarding the dimensioning (cp. to [21], [24], [48]), but the result is quite robust to signal variations.

2)
The disadvantage of overdimensioning can be mitigated if there is no adequate single storage technology for the chosen application in terms of specific power $\omega$. A HESS can meet the required specific power in this typical case by assembling two storage technologies with a lower and higher specific power $\omega$ (cp. Section IV-C).

3)
A filter-controlled HESS highly benefits from storage technologies with distinct loss model parameters $\eta$ and $\tau$, i.e., a base storage with low self-discharge rate $\tau_b$ and a peak storage with high efficiency $\eta_p$. This combination may even outperform a well-suited single storage system with a balanced loss model parameterization in terms of losses $L$ and energy capacity $E$ (cp. Section V-C).

In other words, it is proven under the assumption of linear loss models that a hybrid system can reduce total losses $L$ and dimensioning $E$ and $P$ if and only if the storages utilize different loss model parameterization $\eta$ and $\tau$. If not, frequency-based control leads to higher dimensioning $E$ and $P$ and losses $L$ than theoretically possible and do not allocate power optimally (cp. Section V-C) (cp. to [21], [24], [48]).

4)
Lower cutoff frequencies of the filter reduce rated power $P_b$, specific power $\omega_b$, and cycles $C_b$ of the base storage. However, the cutoff frequency barely affects the needed energy capacity $E_b$ by this parameter and the energy capacity $E_h$ of the hybrid system (cp. Section IV-C).

5)
The required rated power $P_p$ of the peak storage approximately matches the required rated power of the single storage $E_s$ for lower and medium cutoff frequencies $f_c$. Only the base storage rated power $P_b$ decreases towards lower cutoff frequencies $f_c$ (cp. Section IV-C).

6)
The advantages of a hybrid system increase for signals with an emphasis on high frequencies (cp. Section V-A).

7)
The advantages of a hybrid system diminish for signals with a high mean value offset as the results for the base storage converge to the results of the single storage, making an extra peak storage superfluous (cp. Section V-B).

8)
Higher feedback factors $k$ decrease the energy capacity $E_p$ of the peak storage by increasing the energy capacity $E_b$ of the base storage. The total capacity $E_h$ of the hybrid system stays approximately constant. Both effects increase the spread in specific powers $\omega$ of the base and peak storage, making the feedback factor $k$ a significant design variable to tune the resulting specific powers $\omega$ to existing storage technologies (cp. Section V-D). An open loop control without feedback provides poor performance and high standard deviation and is therefore not recommended (cp. Section V-D).

### B. DESIGN GUIDELINES

It is advised to use optimization techniques to find the best parameters of the filter-based control strategy for a specific application. Otherwise, the parameters can be tuned manually with the help of the following guidelines:

- Use filter-based control only for input signals with low mean value and with an emphasis on high frequencies (cp. Section VI-A-6 and Section VI-A-7)
- Use a base storage with a low self-discharge rate $\tau_b$ and a peak storage with high efficiency $\eta_p$ (cp. Section VI-A-3).
- Choose a low cutoff frequency $f_c$, i.e. 1 % to 10 % of the maximum frequency $f_{max}$ of the input signal, to reduce the power rating $P_b$ of the base storage (cp. Section VI-A-5).
- Choose a feedback factor of $k > 0$. Iteratively adapt this value to match the specific power $\omega_b$ and $\omega_p$ of the chosen storage technologies (cp. Section VI-A-2). Increase the value if the simulation results yield a base storage with a specific power $\omega_b$ that is higher than the chosen base storage technology or if the simulations yield a peak storage with a specific power $\omega_p$ that is lower than the chosen peak storage technology. Decrease the value if the opposite is true. Also, consider adapting the cutoff frequency $f_c$. Decrease it if the yielded specific powers $\omega$ of both storages are too high and increase it if the opposite is true.

## VII. SUMMARY

Hybrid energy storage systems (HESS) are a promising solution for storage problems, and a filter-controlled HESS is a standard implementation as it provides robust results and easy implementation. However, more advanced strategies may provide better performance.

This paper intends to structure, specify, clarify, summarize and provide mathematical background and guidelines to previous work for filter-based control of HESS. The present work builds on a simple linear storage model with efficiency

and self-discharge rate and a carefully conducted simulation setup for numerical experiments with statistical analysis. Results are quantified and normalized. The investigated output characteristics involve energy capacity, power rating, specific power, cycles, dynamic stress and conversion, and self-discharge losses. The influence on these characteristics is investigated for the following design variables: frequency spectrum and mean value of the input signal, cutoff frequency and feedback factor of the control strategy, and parameterization of the loss model of the storage.

The paper proves that a filter-controlled HESS enhances the lifetime of the supported storage but also reveals inherent overdimensioning of the HESS compared to more advanced control strategies. However, it demonstrates that a HESS's dimensions and overall losses can fall below that of a single storage system, assuming storages with distinct efficiency and self-discharge rate parameters. Moreover, the present work shows that a HESS is more effective for high-frequency signals and less effective for signals with high mean value offsets. The feedback factor of the control strategy is shown to be the most prominent design variable.

Potential future work could verify the results experimentally, conduct a similarly structured comparison of filter-based control to other control paradigms or compare different subtypes of filter-based control comprehensively.

## REFERENCES


[1] L. W. Chong, Y. W. Wong, R. K. Rajkumar, R. K. Rajkumar, and D. Isa, "Hybrid energy storage systems and control strategies for stand-alone renewable energy power systems," *Renew. Sustain. Energy Rev.*, vol. 66, pp. 174–189, Dec. 2016.

[2] A. Kuperman and I. Aharon, "Battery–ultracapacitor hybrids for pulsed current loads: A review," *Renew. Sustain. Energy Rev.*, vol. 15, no. 2, pp. 981–992, 2011.

[3] R. Hemmati and H. Saboori, "Emergence of hybrid energy storage systems in renewable energy and transport applications—A review," *Renew. Sustain. Energy Rev.*, vol. 65, pp. 11–23, Nov. 2016.

[4] V. K. R. Kasimalla and V. Velisala, "A review on energy allocation of fuel cell/battery/ultracapacitor for hybrid electric vehicles," *Int. J. Energy Res.*, vol. 42, no. 14, pp. 4263–4283, Nov. 2018.

[5] J. He, C. Shi, T. Wei, X. Peng, and Y. Guan, "Hierarchical optimal energy management strategy of hybrid energy storage considering uncertainty for a 100% clean energy town," *J. Energy Storage*, vol. 41, Sep. 2021, Art. no. 102917.

[6] R. S. Sankarkumar and R. Natarajan, "Energy management techniques and topologies suitable for hybrid energy storage systemphpowered electric vehicles: An overview," *Int. Trans. Electr. Energy Syst.*, vol. 31, Apr. 2021, Art. no. e12819.

[7] T. S. Babu, K. R. Vasudevan, V. K. Ramachandaramurthy, S. B. Sani, S. Chemud, and R. M. Lajim, "A comprehensive review of hybrid energy storage systems: Converter topologies, control strategies and future prospects," *IEEE Access*, vol. 8, pp. 148702–148721, 2020.

[8] S. Hajiaghasi, A. Salemnia, and M. Hamzeh, "Hybrid energy storage system for microgrids applications: A review," *J. Energy Storage*, vol. 21, pp. 543–570, Feb. 2019.

[9] G. A. Ramos and R. Costa-Castelló, "Energy management strategies for hybrid energy storage systems based on filter control: Analysis and comparison," *Electronics*, vol. 11, no. 10, p. 1631, May 2022.

[10] R. Xiong, H. Chen, C. Wang, and F. Sun, "Towards a smarter hybrid energy storage system based on battery and ultracapacitor—A critical review on topology and energy management," *J. Cleaner Prod.*, vol. 202, pp. 1228–1240, Nov. 2018.

[11] T. Sutikno, W. Arsadiando, A. Wangsupphaphol, A. Yudhana, and M. Facta, "A review of recent advances on hybrid energy storage system for solar photovoltaics power generation," *IEEE Access*, vol. 10, pp. 42346–42364, 2022.

[12] Z. A. Thoker and S. A. Lone, "Dynamic performance improvement of wind-diesel power system through robust sliding mode control of hybrid energy storage system," *Wind Eng.*, vol. 46, no. 4, pp. 1065–1079, Aug. 2022.

[13] M. A. Zdiri, T. Guesmi, B. M. Alshammari, K. Alqunun, A. Almalaq, F. B. Salem, H. H. Abdallah, and A. Toumi, "Design and analysis of sliding-mode artificial neural network control strategy for hybrid PV-battery-Supercapacitor system," *Energies*, vol. 15, no. 11, p. 4099, Jun. 2022.

[14] M. Arslan, I. Ahmad, M. K. Azeem, and M. Liaquat, "Dual-stage adaptive control of hybrid energy storage system for electric vehicle application," *J. Energy Storage*, vol. 43, Nov. 2021, Art. no. 103165.

[15] S. A. G. K. Abadi, S. I. Habibi, T. Khalili, and A. Bidram, "A model predictive control strategy for performance improvement of hybrid energy storage systems in DC microgrids," *IEEE Access*, vol. 10, pp. 25400–25421, 2022.

[16] D. Deepika and N. Singh, "Exponential state observer based finite time control of fully active hybrid energy storage system," *Sādhanā*, vol. 47, no. 1, p. 21, Mar. 2022.

[17] H. F. Ghavidel and S. M. Mousavi-G, "Observer-based type-2 fuzzy approach for robust control and energy management strategy of hybrid energy storage systems," *Int. J. Hydrogen Energy*, vol. 47, no. 33, pp. 14983–15000, Apr. 2022.

[18] J. Li, F. Yao, Q. Yang, Z. Wei, and H. He, "Variable voltage control of a hybrid energy storage system for firm frequency response in the U.K." *IEEE Trans. Ind. Electron.*, vol. 69, no. 12, pp. 13394–13404, Dec. 2022.

[19] X. Chen, M. Shi, J. Zhou, Y. Chen, W. Zuo, J. Wen, and H. He, "Distributed cooperative control of multiple hybrid energy storage systems in a DC microgrid using consensus protocol," *IEEE Trans. Ind. Electron.*, vol. 67, no. 3, pp. 1968–1979, Mar. 2020.

[20] Q. Xu, C. Zhang, Z. Xu, P. Lin, and P. Wang, "A composite finite-time controller for decentralized power sharing and stabilization of hybrid fuel cell/supercapacitor system with constant power load," *IEEE Trans. Ind. Electron.*, vol. 68, no. 2, pp. 1388–1400, Feb. 2021.

[21] Y. Jiao and D. Månsson, "A study of the energy exchange within a hybrid energy storage system and a comparison of the capacities, lifetimes, and costs of different systems," *Energies*, vol. 14, no. 21, p. 7045, Oct. 2021.

[22] D. B. W. Abeywardana, B. Hredzak, V. G. Agelidis, and G. D. Demetriades, "Supercapacitor sizing method for energy-controlled filter-based hybrid energy storage systems," *IEEE Trans. Power Electron.*, vol. 32, no. 2, pp. 1626–1637, Feb. 2017.

[23] H.-L.-T. Nguyen, B.-H. Nguyen, T. Vo-Duy, and J. P. F. Trovão, "A comparative study of adaptive filtering strategies for hybrid energy storage systems in electric vehicles," *Energies*, vol. 14, no. 12, p. 3373, Jun. 2021.

[24] S. East and M. Cannon, "Optimal power allocation in battery/supercapacitor electric vehicles using convex optimization," *IEEE Trans. Veh. Technol.*, vol. 69, no. 11, pp. 12751–12762, Nov. 2020.

[25] C. R. Arunkumar, U. B. Manthati, and P. Srinivas, "Accurate modelling and analysis of battery–supercapacitor hybrid energy storage system in DC microgrid systems," *Energy Syst.*, vol. 13, no. 4, pp. 1055–1073, Jul. 2021.

[26] Y. Wu, Z. Huang, H. Liao, B. Chen, X. Zhang, Y. Zhou, Y. Liu, H. Li, and J. Peng, "Adaptive power allocation using artificial potential field with compensator for hybrid energy storage systems in electric vehicles," *Appl. Energy*, vol. 257, Jan. 2020, Art. no. 113983.

[27] S. K. Kollimalla, M. K. Mishra, and N. L. Narasamma, "Design and analysis of novel control strategy for battery and supercapacitor storage system," *IEEE Trans. Sustain. Energy*, vol. 5, no. 4, pp. 1137–1144, Oct. 2014.

[28] N. R. Tummuru, M. K. Mishra, and S. Srinivas, "Dynamic energy management of hybrid energy storage system with high-gain PV converter," *IEEE Trans. Energy Convers.*, vol. 30, no. 1, pp. 150–160, Mar. 2015.

[29] E. Schaltz, A. Khaligh, and P. O. Rasmussen, "Influence of battery/ultracapacitor energy-storage sizing on battery lifetime in a fuel cell hybrid electric vehicle," *IEEE Trans. Veh. Technol.*, vol. 58, no. 8, pp. 3882–3891, Oct. 2009.

[30] H. Liao, J. Peng, Y. Wu, H. Li, Y. Zhou, X. Zhang, and Z. Huang, "Adaptive split-frequency quantitative power allocation for hybrid energy storage systems," *IEEE Trans. Transport. Electrific.*, vol. 7, no. 4, pp. 2306–2317, Dec. 2021.

[31] E. M. Asensio, G. A. Magallán, C. H. De Angelo, and F. M. Serra, "Energy management on battery/ultracapacitor hybrid energy storage system based on adjustable bandwidth filter and sliding-mode control," *J. Energy Storage*, vol. 30, Aug. 2020, Art. no. 101569.

[32] H. Chen, Z. Zhang, C. Guan, and H. Gao, "Optimization of sizing and frequency control in battery/supercapacitor hybrid energy storage system for fuel cell ship," *Energy*, vol. 197, Apr. 2020, Art. no. 117285.
[33] L. Zhang, X. Hu, Z. Wang, F. Sun, J. Deng, and D. G. Dorrell, "Multiobjective optimal sizing of hybrid energy storage system for electric vehicles," *IEEE Trans. Veh. Technol.*, vol. 67, no. 2, pp. 1027–1035, Feb. 2018.
[34] H. Li, T. Yao, X. Zhang, F. Bu, and L. Weng, "Hybrid energy storage management strategy for electric propulsion aircraft based on three-step power distribution," *World Electr. Vehicle J.*, vol. 12, no. 4, p. 209, Oct. 2021.
[35] X. Gao and L. Fu, "SOC optimization based energy management strategy for hybrid energy storage system in vessel integrated power system," *IEEE Access*, vol. 8, pp. 54611–54619, 2020.
[36] S. Tang, X. Huang, Q. Li, N. Yang, Q. Liao, and K. Sun, "Optimal sizing and energy management of hybrid energy storage system for high-speed railway traction substation," *J. Electr. Eng. Technol.*, vol. 16, no. 3, pp. 1743–1754, May 2021.
[37] M. Masih-Tehrani, M. R. Ha'Iri Yazdi, V. Esfahanian, M. Dahmardeh, and H. Nehzati, "Wavelet-based power management for hybrid energy storage system," *J. Modern Power Syst. Clean Energy*, vol. 7, no. 4, pp. 779–790, Jul. 2019.
[38] J. Cao, W. Du, H. Wang, and M. McCulloch, "Optimal sizing and control strategies for hybrid storage system as limited by grid frequency deviations," *IEEE Trans. Power Syst.*, vol. 33, no. 5, pp. 5486–5495, Feb. 2018.
[39] X. Wu, S. Li, S. Gan, and C. Hou, "An adaptive energy optimization method of hybrid battery-supercapacitor storage system for uncertain demand," *Energies*, vol. 15, no. 5, p. 1765, Feb. 2022.
[40] N.-D. Nguyen, C. Yoon, and Y. I. Lee, "A standalone energy management system of battery/supercapacitor hybrid energy storage system for electric vehicles using model predictive control," *IEEE Trans. Ind. Electron.*, early access, Jul. 1, 2022, doi: 10.1109/TIE.2022.3186369.
[41] W. Jiang, L. Zhang, H. Zhao, H. Huang, and R. Hu, "Research on power sharing strategy of hybrid energy storage system in photovoltaic power station based on multi-objective optimisation," *IET Renew. Power Gener.*, vol. 10, no. 5, pp. 575–583, May 2016.
[42] H. Unbehauen, *Regelungstechnik. 1. Klassische Verfahren zur Analyse und Synthese linearer kontinuierlicher Regelsysteme, Fuzzy-Regelsysteme*. Wiesbaden, Germany: Vieweg+Teubner, 2008.
[43] Q. Zhang and G. Li, "Experimental study on a semi-active battery-supercapacitor hybrid energy storage system for electric vehicle application," *IEEE Trans. Power Electron.*, vol. 35, no. 1, pp. 1014–1021, Jan. 2020.
[44] L. W. Chong, Y. W. Wong, R. K. Rajkumar, and D. Isa, "An optimal control strategy for standalone PV system with battery-supercapacitor hybrid energy storage system," *J. Power Sources*, vol. 331, pp. 553–565, Nov. 2016.
[45] A. Jaafar, C. R. Akli, B. Sareni, X. Roboam, and A. Jeunesse, "Sizing and energy management of a hybrid locomotive based on flywheel and accumulators," *IEEE Trans. Veh. Technol.*, vol. 58, no. 8, pp. 3947–3958, Oct. 2009.
[46] Y. Jiao and D. Månsson, "Study of the oversized capacity and the increased energy loss of hybrid energy storage systems and design of an improved controller based on the low-pass filter," *J. Energy Storage*, vol. 50, Jun. 2022, Art. no. 104241.
[47] P. H. Tiemann, A. Bensmann, V. Stuke, and R. Hanke-Rauschenbach, "Electrical energy storage for industrial grid fee reduction—A large scale analysis," *Energy Convers. Manage.*, vol. 208, Mar. 2020, Art. no. 112539.
[48] S. Günther, A. Bensmann, and R. Hanke-Rauschenbach, "Theoretical dimensioning and sizing limits of hybrid energy storage systems," *Appl. Energy*, vol. 210, pp. 127–137, Jan. 2018.
[49] C. Zhao, H. Yin, Z. Yang, and C. Ma, "A quantitative comparative study of efficiency for battery-ultracapacitor hybrid systems," in *Proc. 40th Annu. Conf. Ind. Electron. Soc. (IECON)*, Oct. 2014, pp. 3076–3082.
[50] M. Pang, Y. Shi, W. Wang, and S. Pang, "Optimal sizing and control of hybrid energy storage system for wind power using hybrid parallel PSO-GA algorithm," *Energy Explor. Exploitation*, vol. 37, no. 1, pp. 558–578, Jan. 2019.

**SEBASTIAN GÜNTHER** was born in Halle (Saale), Germany, in 1991. He received the B.Sc. and M.Sc. degrees in mechatronics from Otto-von-Guericke University Magdeburg, Germany, in 2012 and 2014, respectively. He is currently pursuing the Ph.D. degree in electrical engineering with Leibniz University Hannover, Germany.

Since 2015, he has been a Research Assistant with the Section for Electric Energy Storage Systems, Leibniz University Hannover. His research interests include modeling and design of hybrid energy storage systems and energy systems in general and flywheels.

**LEONHARD WEBER** was born in Göttingen, Germany, in 1996. He received the B.Sc. degree in mechanical engineering from Leibniz University Hannover, Germany, in 2019, where he is currently pursuing the M.Sc. degree.

During his studies, he worked as a Student Assistant in different institutes including the Institute of Electric Power Systems, Leibniz University Hannover. His research interests mainly comprise computer science and robotics.

**ASTRID L. BENSMANN** was born in Hamburg, Germany, in 1984. She received the B.Sc. degree in general engineering science from the Hamburg University of Technology, Germany, in 2007, and the Diploma degree in systems engineering and engineering cybernetics and the Ph.D. degree in process and systems engineering from Otto-von-Guericke University Magdeburg, Germany, in 2009 and 2016, respectively.

From 2009 to 2014, she was a Research Assistant with the Chair of Systems Engineering, Magdeburg, Germany. Since 2014, she has been working as a Senior Researcher and a Group Leader with the Section for Electric Energy Storage Systems, Hannover, Germany. Her research interests include modeling, design and operation of energy systems, characterization and operation of battery systems.

**RICHARD HANKE-RAUSCHENBACH** was born in Leipzig, Germany, in 1978. He received the Dipl.-Ing. degree in energy engineering from the Leipzig University of Applied Sciences, Germany, in 2001, and the Ph.D. degree in process engineering from Otto-von-Guericke University Magdeburg, Germany, in 2007.

From 2007 to 2014, he was a Senior Scientist and a Team Leader with the Max Planck Institute for Dynamics of Complex Technical Systems, Magdeburg, Germany. He has received appointments from University Bayreuth, Germany; University Stuttgart, Germany; and Leibniz University Hannover, Germany. Since 2014, he has been a Full Professor at Leibniz University Hannover, Germany, holding the Chair for electric energy storage systems. He has authored and coauthored over 90 articles in international journals and over 80 conference contributions and two book contributions. His research interests include electric energy storage systems, vehicle energy systems, multimodal energy systems, power to gas, and PEM water electrolysis.